PREPRINT

Thermophysical and mechanical properties of LaB_6 and CeB_6 synthesized through spark plasma sintering

Yifan Sun[a,b], Yuji Ohishi[a], Junya Higaki[a], Hiroaki Muta[a], and Ken Kurosaki[b,c]

[a]Graduate School of Engineering, Osaka University, Suita, Osaka 565-0871, Japan;[b]Institute for Integrated Radiation and Nuclear Science, Kyoto University, Kumatori, Osaka 590-0494, Japan;[c]Research Institute of Nuclear Engineering, University of Fukui, Tsuruga, Fukui 914-0055, Japan

ARTICLE HISTORY
Compiled May 10, 2023

ABSTRACT
Following the Fukushima Daiichi nuclear power plant accident in 2011, the development of accident tolerant fuels (ATFs) has become an integral part of the promotion of nuclear safety. Of the many design criteria, a high thermal conductivity reduces a fuel pellet's peak temperature and radial temperature gradient. Although various uranium borides such as UB_2 and UB_4 are promising ATFs that have high-temperature stability, high uranium density, and good thermal conductivity, little is known about UB_6, as it has yet to be fabricated under normal conditions. As a metal hexaboride, UB_6 may have excellent electrical conductivity, likely giving it a much higher thermal conductivity than that of UO_2. In this work, we investigate the thermophysical and mechanical properties of non-radioactive LaB_6 and CeB_6 to estimate the potential properties of UB_6, as it has yet to be successfully fabricated. The thermophysical properties of UB_6 are compared with those of UO_2, UB_2, and UB_4 to help clarify whether future attempts at fabricating UB_6 under high pressure or with other dopants are worthwhile for the development of ATFs.

KEYWORDS
Thermal conductivity; electrical conductivity; Vickers hardness; Elastic properties; LaB_6; CeB_6; nuclear fuel

1. Introduction

UO_2 has long been used as the primary nuclear fuel because of its thermal stability at high temperatures and uranium density. Following the Fukushima Daiichi nuclear power plant accident in 2011, the U.S. Department of Energy sped up the development of accident-tolerant fuel-cladding systems that can withstand harsh conditions during loss-of-coolant accidents (LOCA) and that can outperform standard UO_2-zircaloy systems during normal operations[1]. Enhanced cladding oxidation resistance, reduced fuel-cladding interactions, and improved fission product retention within the fuel are some of the top design priorities, and these ATFs must also be compatible with current fuel pellet manufacturing protocols and reactor designs[1–3]. Over the past few years, various ATFs such as uranium silicate, uranium nitride, uranium boride, and

Corresponding author. Email: yifan.sun.7r@kyoto-u.ac.jp
Corresponding author. Email: kurosaki.ken.6n@kyoto-u.ac.jp

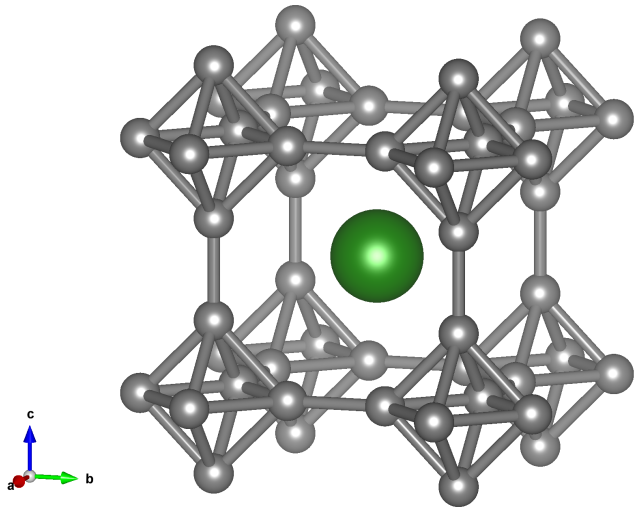

Figure 1. Crystal structure of metal hexaborides. One metal atom is surrounded by eight B_6 octahedra.

UO_2 composites with high thermal conductivities have been investigated [4–10]. ATFs with high thermal conductivity enhance the safety of nuclear power plants by reducing the fuel's temperature and lowering its radial temperature gradient[11]. Among the ATF candidates, UO_2–UB_x composites have attracted considerable attention because uranium borides may act as burnable poisons without sacrificing the fuel's thermal conductivity, as is the case when adding Gd_2O_3 to UO_2[7]. In addition, the boron isotopes B^{10} and B^{11} have significantly different neutron absorption cross-sections, which provides better control over the fuel's reactivity. The fabrication of dense UB_2, UB_4, UB_2-UO_2, and UB_4-UO_2 pellets have been recently reported by Kardoulaki et al.[7,12]; above 1000 K, the thermal conductivities of UB_2 and UB_4 are an order higher than that of UO_2[7,13]. The UO_2-UB_x composites also showed improved thermal diffusivity over that of pure UO_2[12].

Unlike UB_2 and UB_4, little is known about the thermophysical properties of UB_6, as it has yet to be fabricated under normal conditions. The unit cells of metal hexaborides have a cubic-CsCl structure with a metal atom surrounded by eight B_6 octahedra, as shown in Fig.1[14]. Although the majority of known actinides (Np, Pu, Am) can form hexaborides, the inability of uranium to form hexaboride is thought to be related to its small effective radius[15,16]. Similarly, small rare earth elements from Ho to Lu do not form hexaborides because the metal atom's site within the boron sublattice of MB_6 is much larger than that of MB_4 and MB_{12}, and the boron octahedra "cage" of MB_6 is quite inflexible[15]. In order to stabilize MB_6 with small metal atoms, previous researchers introduced bigger metal ions such as La^{3+} or Yb^{3+} and successfully synthesized solid solutions such as (Tm,La)B_6 and (Ho,La)B_6[17–19]. Therefore, although UB_6 has yet to be synthesized under normal conditions, it has been proposed that its fabrication is possible by forming solid solutions with hexaborides such as ThB_6 [15,20].

Metal hexaborides have interesting electrical properties depending on the valency of the metal atom. In general, the metal atom must be at least divalent to donate

two electrons to stabilize the electron-deficient boron octahedron[15]. These two electrons and the 18 valence electrons of the B_6 octahedron fill the valence band of MB_6 [21–23], meaning that divalent hexaborides such as CaB_6 are semiconductors/semimetals. MB_6 such as trivalent hexaborides and tetravalent hexaborides with additional electrons are metallic after the 20-electron valence band is filled and have much higher electrical conductivities than those of divalent hexaborides[15,22,24,25]. Because the known actinide hexaborides such as PuB_6, NpB_6, and ThB_6 are not divalent hexaborides[26], we speculate that, if fabricated, UB_6 could show excellent electrical conductivity. As electronic thermal conductivity cannot be ignored in metals, the contribution of UB_6 electrons to its heat transport should result in a much higher thermal conductivity than that of UO_2. Therefore, it is postulated that UB_6 can be used in UB_x-UO_2 composite fuel just like UB_2 and UB_4.

Because the fabrication of UB_6 is challenging, we first investigated the thermophysical properties of non-radioactive surrogates LaB_6 and CeB_6 to gain some insight into the properties of the hypothetical compound UB_6. LaB_6 and CeB_6 are chosen because they are classified as metallic multivalent hexaborides, just like UB_6. As a result, it is expected that the electrical properties of LaB_6 and CeB_6 are similar to that of UB_6. Furthermore, these metal hexaborides share an identical crystal structure which should result in comparable elastic properties. Herein, dense LaB_6 and CeB_6 pellets are fabricated via spark plasma sintering, and the two surrogates' thermophysical properties are measured to help determine whether it is worth pursuing UB_6's fabrication as an ATF candidate.

2. Experimental methods

Bulk LaB_6 and CeB_6 samples were prepared by spark plasma sintering (SPS) LaB_6 (2N, Kojundo Chemicals) and by using CeB_6 (2N, Kojundo Chemicals) powders, respectively. The samples were sintered at 1700°C and held at a pressure of 100 MPa for 10 min under Ar gas flow (0.2 L/min, 6N, Air Liquide). The phases of the sintered samples were investigated using X-ray diffraction (XRD) from 2θ=20°–120° (CuKα radiation, Ultima-IV, Rigaku), and the lattice parameters were calculated using the least-squares method. Element distribution within the pellets was evaluated through scanning electron microscopy and energy dispersive spectroscopy (SEM-EDS).

The electrical conductivity of the samples was measured using a DC four-probe method (ULVAC ZEM-3) in a He atmosphere. The thermal diffusivity was measured using a laser flash technique (LFA 457 Microflash, Netzsch) under Ar gas flow (0.2 L/min, 6N, Air Liquide) from 298 to 1273 K. Laser flash measurements were repeated three times at each temperature. The thermal conductivity κ_{tot} of the samples was calculated from thermal diffusivity α, density ρ, and specific heat C_p using the following equation:

$$\kappa_{tot} = \alpha \rho C_p \tag{1}$$

The contributions of electrons and phonons to heat transport were calculated using

$$\kappa_{ele} = L\sigma T \tag{2}$$

$$\kappa_{lat} = \kappa_{tot} - \kappa_{ele} \tag{3}$$

where L is the Lorenz number, σ is the electrical conductivity, and T is the tem-

Table 1. Lattice parameters of the prepared LaB_6 and CeB_6 bulk samples.

Sample	a=b=c, nm	Comment
LaB_6	0.4153	This work
	0.4157	[27]
CeB_6	0.4139	This work
	0.4140	[28]

perature. The Lorenz number is assumed to be 2.44×10^{-8} $W\Omega K^{-2}$ and temperature-independent.

The longitudinal and transverse sound velocities of the samples were measured using a pulse-echo method with a digital oscilloscope (9310A, LeCory) to calculate the elastic properties. Three separate measurements were conducted with each sample. Finally, the microhardness of the samples was measured using a Vickers hardness tester (HMV-G20, Shimadzu) under a load of 0.98 N and holding time of 10 s. The indentation experiment was repeated 10 times for each sample.

3. Results and Discussion

3.1. XRD & SEM-EDS analyses

Fig.2 shows the XRD patterns of the bulk LaB_6 and CeB_6 samples prepared by SPS. The diffraction peaks of the samples were in agreement with reference data[27,28], and no impurity phases were present, confirming that single-phase LaB_6 and CeB_6 were successfully fabricated. In addition, the calculated lattice parameters as shown in Table 1 were in good agreement with the values given in the literature. Fig.2 also shows the sintered pellets and relative densities of the samples as calculated from their measured and theoretical densities. Finally, the SEM-EDS images shown in Fig.3 confirmed that the constituent elements were uniformly distributed in the bulk samples.

3.2. Thermal conductivity

Fig.4 shows the total thermal conductivity of LaB_6 and CeB_6 as calculated using Eq.1 with reference data[7,24,29–31]. The densities of the samples were assumed to be temperature-independent in Eq.1, and the heat capacity data of CeB_6 and LaB_6 were taken from the existing literature[32,33]. As the heat capacity of LaB_6 was only reported up to 1000 K, its value was assumed to be constant after 1000 K during the calculation.

The thermal conductivity of CeB_6 at high temperatures has not been previously reported, and our data suggested that its value is weakly temperature-dependent (i.e., approximately 45 $Wm^{-1}K^{-1}$, from 298 to 1273 K). For LaB_6, only Tanaka [31] previously measured its thermal diffusivity from 1300 to 2000 K using an electron beam modulation technique. The pyrometer used by Tanaka was unable to detect the weak radiation emitted by a sample below 1300 K, and the sputtering of the sample from the electron beam could not be ignored above 2000 K[34]. Therefore, the thermal conductivity of LaB_6 as reported here between 298 and 1273 K fills the gap in the existing literature. At 1273 K, LaB_6 exhibited a thermal conductivity of 54.9 $Wm^{-1}K^{-1}$, which was in good agreement with the data reported by Tanaka ($\sim$ 56 $Wm^{-1}K^{-1}$ at 1300 K) [31]. From 298 to 1273 K, the thermal conductivity of LaB_6 and CeB_6 is on par with

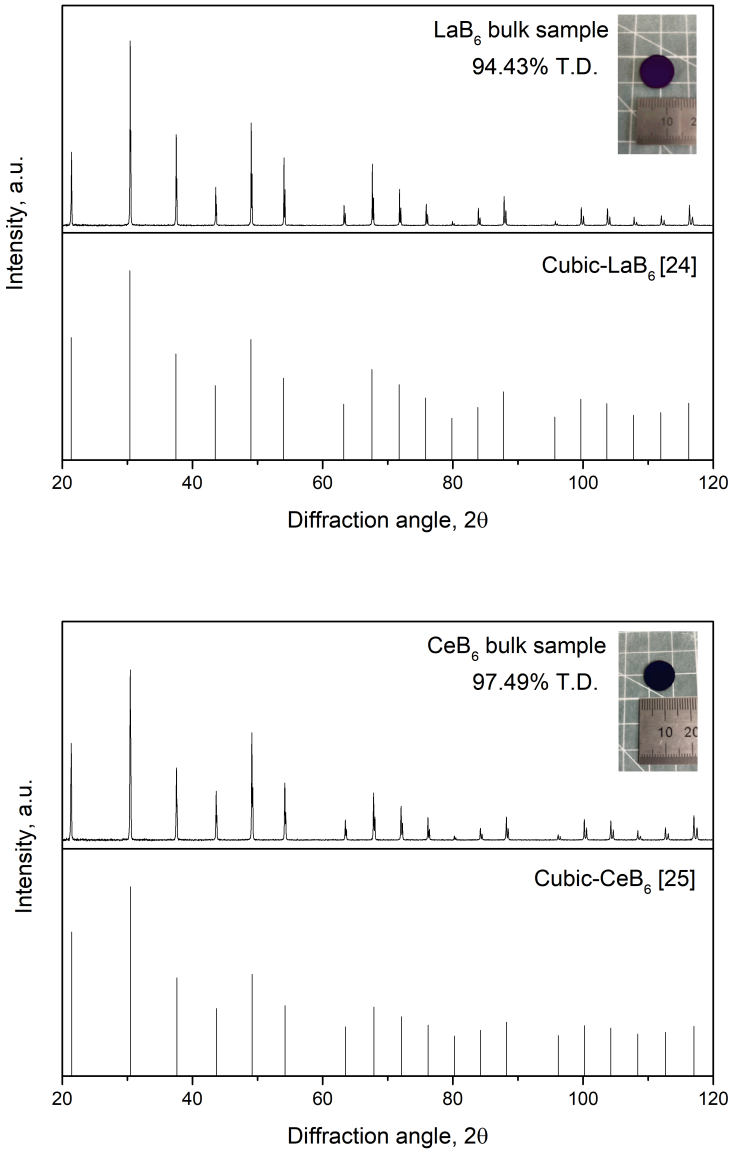

Figure 2. XRD patterns and images of the prepared bulk LaB_6 and CeB_6 samples.

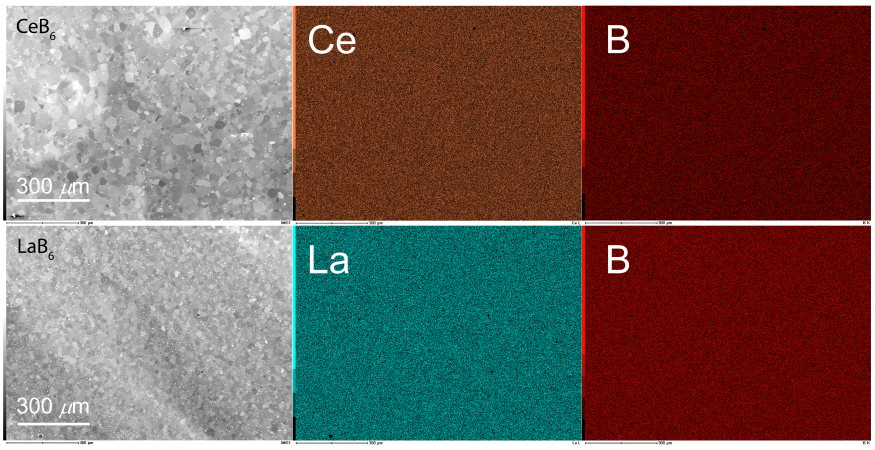

Figure 3. SEM-EDS images of CeB_6 and LaB_6.

good heat conductors such as Fe and Pt[35] and is significantly higher than that of UB_2 and UB_4[7]. This is probably due to a higher contribution from the heat-conducting electrons of MB_6.

Although we might speculate that non-divalent hexaborides are all good heat conductors, results from a first-principle study by Shi et al.[29] have suggested that the thermal conductivity of ThB_6 rapidly declines with temperatures and is therefore much lower than those of LaB_6 and CeB_6. To the best of our knowledge, no studies have been conducted on the thermal conductivity of ThB_6 at high temperatures. However, its electrical conductivity has been investigated by Auskern & Aronson and Samsonov[24,30]. The electronic thermal conductivity of ThB_6 calculated from experimental data was found to be close to 10 times higher than that reported by Shi et al.[29] at 300 K, as shown in Fig.4. A similar observation was made for ThB_4, a metallic tetraboride, in which the electronic thermal conductivity reported by Shi et al.[29] was much less than indicated by experimental data[24]. Although the Lorenz numbers of ThB_4 and ThB_6 may be smaller than the ideal value, the deviation is so large that this seems highly unlikely. It is plausible that the fixed electron–phonon interaction relaxation time of 10^{-15} s as selected by Shi et al.[29] resulted in this underestimation of the electronic thermal conductivity of thorium borides.

3.3. Electrical properties

The electrical conductivity of LaB_6 and CeB_6 was investigated to clarify the sources of their excellent thermal conductivities. The electrical resistivity of LaB_6 and CeB_6 measured using the DC four-probe method are shown in Fig.5 with reference data[31, 36–39]. The electrical resistivity of LaB_6 and CeB_6 obtained in this study from 300 to 1073 K can be expressed as

$$\rho_{LaB_6}(\mu\Omega \cdot \mathrm{cm}) = 10.9 + 4.22 \times 10^{-2}(T - 300) \quad (4)$$

$$\rho_{CeB_6}(\mu\Omega \cdot \mathrm{cm}) = 30.3 + 4.42 \times 10^{-2}(T - 300) \quad (5)$$

The resistivity of LaB_6 obtained in this study was in excellent agreement with that reported by Williams et al.[39]. Zhou et al. prepared nanostructured LaB_6 with smaller grain sizes as compared to the samples used in this work[37]. This may have led to a

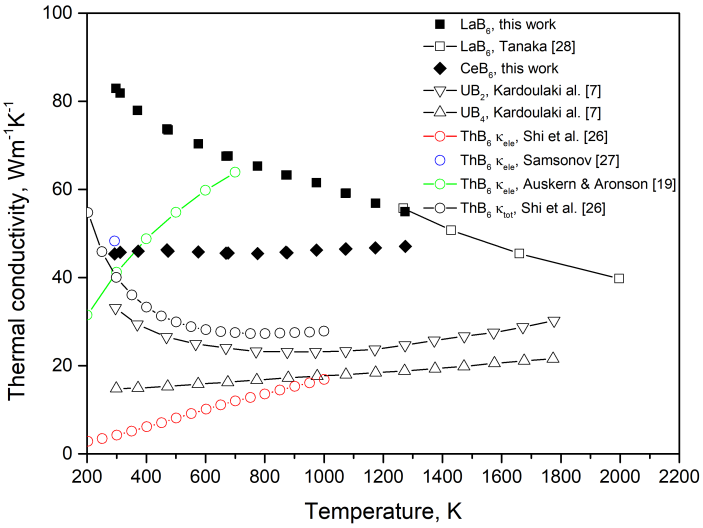

Figure 4. Thermal conductivities of LaB_6, CeB_6, and other metal borides

.

higher electrical resistivity from electron-defect scattering at the grain boundaries. The deviation between this work and that of Tanaka is attributed to the lower accuracy in the sample temperatures reported by Tanaka[31]. As previously mentioned, Tanaka assumed that the emissivity of LaB_6 has a temperature-independent value of 0.8[31], and E. K. Storms later clarified in 1979 that the emissivity of LaB_6 decreases with increasing temperature[40]. The electrical resistivity of CeB_6 reported here was found to be less than those of previous studies[36,38], whereas none of the previous studies were in agreement. The deviation is thought to be related to the characteristics of the fabricated samples (e.g., porosity, grain size, impurities), as the same measurement technique (DC four-probe method with the ULVAC ZEM apparatus) was used. In addition to LaB_6 and CeB_6, excellent electrical conductivity is a common trait of various metallic hexaborides. For example, ThB_6 and NdB_6 have low electrical resistivities of 18 and ~13 $\mu\Omega$·cm at 300 K[24,41], respectively. Compared with the electrical resistivity of UB_4 (i.e., 370 $\mu\Omega$·cm at 300 K[42]), those of metallic hexaborides are one order of magnitude less. For UB_2, its electrical resistivity has been measured only for single crystals, and that of UO_2 is several orders of magnitude higher[43,44].

Fig.6 shows the contributions of electrons and phonons to the total thermal conductivity of LaB_6 and CeB_6 as calculated by the Wiedemann–Franz law. For LaB_6, assuming a temperature-independent Lorenz number above 1000 K is no longer valid, as it leads to a negative lattice thermal conductivity. The Lorenz number of LaB_6 may also be less than 2.44×10^{-8} $W\Omega K^{-2}$. Fig.6 clearly shows that the excellent thermal conductivity of LaB_6 and CeB_6 was the result of the overwhelming contribution of their free electrons in heat transport. Therefore, we postulated that unless UB_6 is an outlier, without the metallic behavior prevalent in non-divalent hexaborides, UB_6 should have a superior thermal conductivity over that of UO_2 and even ATF candidates such as UB_2 and UB_4.

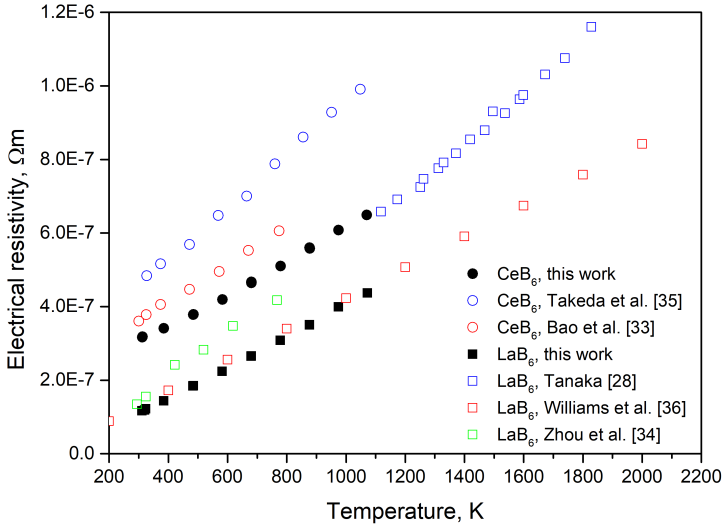

Figure 5. Electrical resistivities of various metal hexaborides.

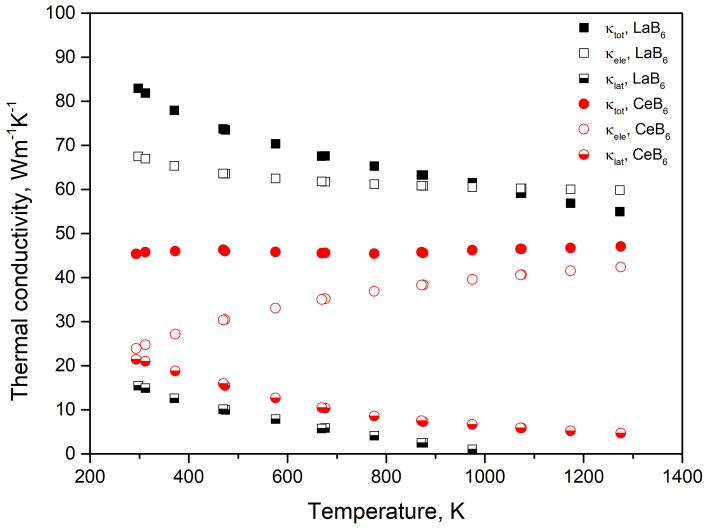

Figure 6. Total, electronic, and lattice thermal conductivities of LaB_6 and CeB_6.

Table 2. Elastic properties of LaB_6, CeB_6, and UO_2.

Material	V_l, m s^{-1}	V_s, m s^{-1}	θ_D, K	B, GPa	G, GPa	E, GPa	ν	Ref
LaB_6	8447	5185	785	158	120	287	0.20	This work
	-	-	773	163	129	307	0.20	[47]
CeB_6	8293	5001	761	166	117	284	0.21	This work
	-	-	751	182	127	308	0.22	[48]
UO_2	-	-	384	202.1	83.1	219.3	0.319	[49]

3.4. Elastic properties

Various elastic properties such as Shear modulus G, Young's modulus E, Bulk modulus B, Poisson's ratio ν, and Debye temperature θ_D were calculated based on the sound velocities of samples using the following equations[45,46]:

$$G = \rho V_s^2 \tag{6}$$

$$E = \frac{G(3V_l^2 - 4V_s^2)}{(V_l^2 - V_s^2)} \tag{7}$$

$$B = \rho(V_l^2 - \frac{4}{3}V_s^2) \tag{8}$$

$$\nu = \frac{1}{2}\frac{V_l^2 - 2V_s^2}{V_l^2 - V_s^2} \tag{9}$$

$$\theta_D = (\frac{\mathrm{h}}{\mathrm{k_B}})[\frac{9N}{4\pi V_0(V_l^{-3} + 2V_s^{-3})}]^{\frac{1}{3}} \tag{10}$$

where ρ is the density, V_s is the transverse sound velocity, V_l is the longitudinal sound velocity, h is Planck's constant, $\mathrm{k_B}$ is Boltzmann's constant, N is the number of atoms per unit cell, and V_0 is the volume of the unit cell. The derived elastic properties are summarized in Table 2 with reference values[47–49]. Tanaka et al. and Luthi et al.[47,48] provided only the elastic constants of LaB_6 and CeB_6, respectively. Therefore, the referenced elastic properties of LaB_6 and CeB_6 as listed in Table 2 are the calculated Voigt–Reuss–Hill averages from these elastic constants. Overall, the various elastic properties of LaB_6 and CeB_6 calculated from sound velocities in this work were in good agreement with the values in the literature.

For cubic-MB_6, its lattice parameter did not show considerable variation with different metal atoms due to the rigid surrounding boron octahedra[15,25]. In addition, the acoustic branches of the phonon dispersion spectra of different MB_6 have been previously shown to resemble one another[50,51]. Therefore, the elastic properties of LaB_6 and CeB_6 as listed in Table 2 provide a reasonable means of estimating those of UB_6. Compared to UO_2[49], UB_6 should be more resistant against shear transformation and elastic deformation but susceptible to compression, given its potentially smaller bulk modulus.

3.5. Vickers hardness and fracture toughness

The Vickers hardness and fracture toughness of the LaB_6 and CeB_6 samples were evaluated using the indentation method, as shown in Fig.7. Niihara's equation for a Palmqvist crack ($0.25 \leq l/a \leq 2.5$) was used to calculate the fracture toughness[52]:

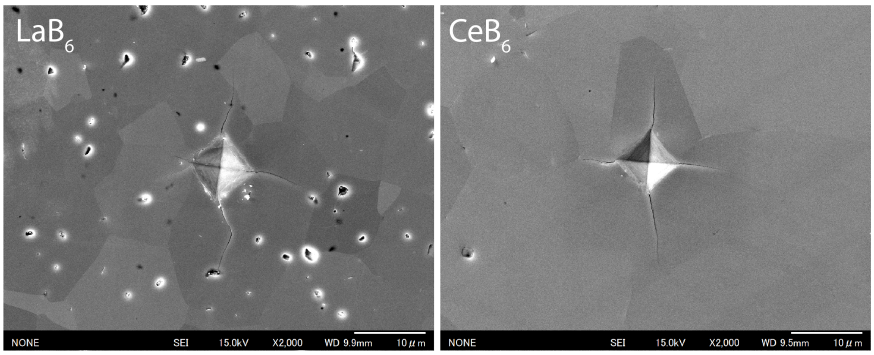

Figure 7. Vickers hardness indentations of LaB_6 and CeB_6.

Table 3. Vickers hardness Hv and fracture toughness K_{IC} of LaB_6, CeB_6, and other nuclear fuels.

Sample	Vickers hardness, GPa	Fracture toughness, MPa·m$^{0.5}$	Applied load, N	Ref
LaB_6	22.06±0.89	2.82±0.15	0.98	This work
	20.34±1	3.02±0.5	0.98	[54]
	18.2	-	5	[56]
	22.3	-	9.8	[37]
CeB_6	19.23±0.19	3.24±0.18	0.98	This work
	14.2	4.6	0.98	[55]
	21.0	2.30	0.294	[57]
	21.2	-	5	[36]
UB_2	22.0±2.9	-	0.015	[7]
UB_4	28.4±1.4	-	0.015	[7]
UO_2	6.21	-	0.98	[53]

$$K_{IC} = 0.0089(\frac{E}{H})^{0.4}\frac{P}{al^{0.5}} \tag{11}$$

where K_{IC} (Pa·m$^{0.5}$) is the fracture toughness, E (GPa) is the elastic modulus, H (GPa) is the Vickers hardness, P (N) is the applied indentation force, a (m) is the half diagonal of the indentation, and l (m) is the length of the propagated crack. The Vickers hardness values shown in Table 3 were obtained under an applied load of 0.98 N, as higher loads resulted in distorted indentations that were unusable.

Metal borides are well-known for their high hardness, and it is no exception that LaB_6 and CeB_6 are much harder than polycrystalline UO_2[53]. The Vickers hardness values of LaB_6 and CeB_6 obtained in this work under a 0.98 N load were 22.06 ± 0.89 and 19.23 ± 0.19 GPa, respectively. Because the hardness measurement is affected by the size of the indentation, only results from indentation experiments under the same applied load could be meaningfully compared. The smaller Vickers hardness of LaB_6 reported by Sonber et al.[54] is thought to be caused by the differences between the preparation methods of the samples. Sonber et al. hot pressed a LaB_6 sample at a higher temperature (1950°C) and longer duration (2 h), which could have resulted in grain growth and lowered the sample's hardness[54]. Regarding the hardness of CeB_6, the deviation between this work and that of Sonber et al.[55] was attributed to the difference in the relative densities of the fabricated samples.

4. Conclusion

In this study, the thermophysical and mechanical properties of UB_6 were investigated by studying those of non-radioactive metal hexaborides such as LaB_6 and CeB_6. The electrical conductivity of LaB_6 and CeB_6 showed metallic behaviors and were one order of magnitude higher than that of UB_4. The large contributions from free electrons to the heat transport in LaB_6 and CeB_6 led to excellent thermal conductivities that were more than 10 times higher than that of UO_2 at temperatures greater than 1000 K. Other mechanical properties of LaB_6 and CeB_6, such as Young's modulus, shear modulus, and hardness, were also determined to be significantly higher than those of UO_2. Based on the properties of LaB_6 and CeB_6 as well as the similarities in the crystal and electronic structures of non-divalent metal hexaborides, we concluded that, if fabricated, UB_6 could be another mechanically robust accident-tolerant fuel with excellent thermal conductivity.

Acknowledgments

This work was supported in part by MEXT/JSPS KAKENHI, grant number JP20K21162, and MEXT Innovative Nuclear Research and Development Program, grant number JPMXD0220.

Disclosure statement

The authors have no competing interests to declare.

Data availability statement

The datasets generated and/or analyzed during this study are available from the corresponding authors on reasonable request.

References

[1] Carmack J, Goldner F, Bragg-Sitton SM, et al. Overview of the US DOE accident tolerant fuel development program. Idaho National Lab.(INL), Idaho Falls, ID (United States); 2013.

[2] Zinkle SJ, Terrani KA, Gehin JC, et al. Accident tolerant fuels for LWRs: A perspective. J Nucl Mater. 2014;448(1-3):374–379.

[3] Karoutas Z, Brown J, Atwood A, et al. The maturing of nuclear fuel: Past to accident tolerant fuel. Prog Nucl Energy. 2018;102:68–78.

[4] White JT, Nelson AT, Dunwoody JT, et al. Thermophysical properties of U_3Si_2 to 1773 k. J Nucl Mater. 2015;464:275–280.

[5] White JT, Travis AW, Dunwoody JT, et al. Fabrication and thermophysical property characterization of UN/U_3Si_2 composite fuel forms. J Nucl Mater. 2017;495:463–474.

[6] Muta H, Kurosaki K, Uno M, et al. Thermal and mechanical properties of uranium nitride prepared by SPS technique. J Mater Sci. 2008;43(19):6429–6434.

[7] Kardoulaki E, White JT, Byler DD, et al. Thermophysical and mechanical property assessment of UB_2 and UB_4 sintered via spark plasma sintering. J Alloys Compd. 2020; 818:153216.

[8] Frazer D, Maiorov B, Carvajal-Nunez U, et al. High temperature mechanical properties of fluorite crystal structured materials (CeO_2, ThO_2, and UO_2) and advanced accident tolerant fuels (U_3Si_2, UN, and UB_2). J Nucl Mater. 2021;554:153035.
[9] Costa DR, Hedberg M, Middleburgh SC, et al. UN microspheres embedded in UO_2 matrix: an innovative accident tolerant fuel. J Nucl Mater. 2020;540:152355.
[10] Gong B, Yao T, Lei P, et al. U_3Si_2 and UO_2 composites densified by spark plasma sintering for accident-tolerant fuels. J Nucl Mater. 2020;534:152147.
[11] Terrani KA, Wang D, Ott LJ, et al. The effect of fuel thermal conductivity on the behavior of LWR cores during loss-of-coolant accidents. J Nucl Mater. 2014;448(1-3):512–519.
[12] Kardoulaki E, Frazer DM, White JT, et al. Fabrication and thermophysical properties of uo2-ub2 and uo2-ub4 composites sintered via spark plasma sintering. Journal of Nuclear Materials. 2021;544:152690.
[13] Wang BT, Zheng JJ, Qu X, et al. Thermal conductivity of UO_2 and PuO_2 from first-principles. J Alloys Compd. 2015;628:267–271.
[14] Momma K, Izumi F. Vesta 3 for three-dimensional visualization of crystal, volumetric and morphology data. Journal of applied crystallography. 2011;44(6):1272–1276.
[15] Etourneau J, Hagenmuller P. Structure and physical features of the rare-earth borides. Philos Mag B. 1985;52(3):589–610.
[16] Eick HA, Mulford R. Americium and neptunium borides. J Inorg Nucl Chem. 1969; 31(2):371–375.
[17] Nichols M, Mar R, Johnson Q. Questions concerning the existence of erbium hexaboride: The crystal structure of (er0. 8ca0. 2) b6. Journal of the Less Common Metals. 1973; 33(2):317–320.
[18] Kasaya M, Iga F, Yashima H, et al. Susceptibility, liii absorption and specific heat across the mixed valence range in r1- xlaxb6 and r1- yybyb6 (r= tm, sm). Journal of Magnetism and Magnetic Materials. 1983;31:389–390.
[19] Berrada A, Mercurio JP, Etourneau J, et al. Synthese et etude cristallochimique et magnetique des solutions solides laxho1- xb6. Materials Research Bulletin. 1976;11(8):947–951.
[20] Matar S, Etourneau J. The electronic structures of uranium borides from local spin density functional calculations. Int J Inorg Mater. 2000;2(1):43–51.
[21] Johnson RW, Daane AH. Electron requirements of bonds in metal borides. J Chem Phys. 1963;38(2):425–432.
[22] Longuet-Higgins HC, Roberts MDV, Randall JT. The electronic structure of the borides MB_6. Proc R Soc Lond, A. 1954;224(1158):336–347.
[23] Lipscomb WN, Britton D. Valence structure of the higher borides. J Chem Phys. 1960; 33(1):275–280.
[24] Auskern A, Aronson S. Electrical properties of thorium borides. J Chem Phys. 1968; 49(1):172–176.
[25] Cahill JT, Graeve OA. Hexaborides: a review of structure, synthesis and processing. J Mater Res Technol. 2019;8(6):6321–6335.
[26] Jain A, Ong SP, Hautier G, et al. Commentary: The materials project: A materials genome approach to accelerating materials innovation. APL Mater. 2013;1(1):011002.
[27] Toby B; 2008. Argonne National Laboratory, Lemont, IL, USA. Private Communication.
[28] Blomberg M, Merisalo M, Korsukova M, et al. X-ray structure refinement of single crystals of Ceb_6 and $Ce_{0.75}La_{0.25}B_6$ solid solution grown by the solution method. J Less-Common Met. 1989;146:309–318.
[29] Shi D, Song J, Qin Y, et al. Evolutionary search for novel thorium borides toward advanced nuclear fuels. J Phys Chem C. 2022;.
[30] Samsonov GV. Plenum press handbooks of high-temperature materials. no. 2. properties index. Plenum Press, Inc., New York; 1964.
[31] Tanaka T. The thermal and electrical conductivities of Lab_6 at high temperatures. J Phys C: Solid State Phys. 1974;7(9):L177.
[32] Muratov V, Bolgar A, Loboda P, et al. Enthalpy and heat capacity of CeB_6, PrB_6 and EuB_6 within wide temperature range. Poroshkovaya Metall. 1988;:70–75.

[33] Ivashchenko V, Turchi P, Shevchenko V, et al. Electronic, thermodynamics and mechanical properties of LaB_6 from first-principles. Physica B. 2018;531:216–222.
[34] Tanaka T, Suzuki H. Thermal conductivity of carbon materials at high temperatures by a modulated electron beam technique. Tokyo Inst. of Tech.; 1972.
[35] Brandes EA, Brook G. Smithells metals reference book. Elsevier; 2013.
[36] Lihong B, Zhang J, Shenlin Z. Effect of particle size on the polycrystalline CeB_6 cathode prepared by spark plasma sintering. J Rare Earths. 2011;29(6):580–584.
[37] Zhou S, Zhang J, Liu D, et al. Synthesis and properties of nanostructured dense LaB_6 cathodes by arc plasma and reactive spark plasma sintering. Acta Mater. 2010;58(15):4978–4985.
[38] Takeda M, Fukuda T, Miura T. Thermoelectric properties of metal-hexaborides. In: Twenty-First International Conference on Thermoelectrics, 2002. Proceedings ICT'02.; IEEE; 2002. p. 173–176.
[39] Williams M, Jackson L, Kippenhan D, et al. Lanthanum hexaboride (Lab_6) resistivity measurement. Appl Phys Lett. 1987;50(25):1844–1845.
[40] Storms EK. The emissivity of LaB_6 at 650 nm. J Appl Phys. 1979;50(6):4450–4450.
[41] Paderno YB, Novikov V, Garf E. Electrical properties of hexaborides of the alkaline-and rare-earth metals at low temperatures. Soviet Powder Metallurgy and Metal Ceramics. 1969;8(11):921–923.
[42] Nishi Y, Arita Y, Matsui T, et al. Thermoelectric properties of UB_5 from 300 to 850 k. J Phys Chem Solids. 2005;66(2-4):652–654.
[43] Yamamoto E, Haga Y, Honma T, et al. De Haas-van Alphen Effect and Energy Band Structure in UB_2. J Phys Soc Jpn. 1998;67(9):3171–3175.
[44] Bates J, Hinman C, Kawada T. Electrical conductivity of uranium dioxide. J Am Ceram Soc. 1967;50(12):652–656.
[45] Edward S, Anderson O, Schreiber S. Elastic constants and their measurement ; 1974.
[46] Anderson OL. A simplified method for calculating the Debye temperature from elastic constants. J Phys Chem Solids. 1963;24(7):909–917.
[47] Tanaka T, Yoshimoto J, Ishii M, et al. Elastic constants of LaB_6 at room temperature. Solid State Commun. 1977;22(3):203–205.
[48] Lüthi B, Blumenröder S, Hillebrands B, et al. Elastic and magnetoelastic effects in CeB_6. Z Phys B. 1984;58(1):31–38.
[49] Kato M, Matsumoto T. Thermal and mechanical properties of UO_2 and Pu_2; 2015.
[50] Serebrennikov D, Clementyev E, Alekseev PA. Analysis of the crystal lattice instability for cage–cluster systems using the superatom model. J Exp Theor Phys. 2016;123(3):452–460.
[51] Kunii S, Effantin JM, Rossat-Mingnod J. Lattice dynamics in Ceb_6 studied by neutron-scattering and specific-heat measurements. J Phys Soc Jpn. 1997;66(4):1029–1032.
[52] Niihara K, Morena R, Hasselman D. Evaluation of K_{IC} of brittle solids by the indentation method with low crack-to-indent ratios. J Mater Sci Lett. 1982;1(1):13–16.
[53] Kurosaki K, Saito Y, Muta H, et al. Nanoindentation studies of UO_2 and (U, Ce)O_2. J Alloys Compd. 2004;381(1-2):240–244.
[54] Sonber J, Sairam K, Murthy TC, et al. Synthesis, densification and oxidation study of lanthanum hexaboride. J Eur Ceram Soc. 2014;34(5):1155–1160.
[55] Sonber J, Murthy TC, Sairam K, et al. Effect of $TiSi_2$ addition on densification of cerium hexaboride. Ceram Int. 2016;42(1):891–896.
[56] Li-Hong B, Jiu-Xing Z, Shen-Lin Z, et al. Preparation and characterization of grain size controlled LaB_6 polycrystalline cathode material. Chin Phys Lett. 2010;27(10):107901.
[57] 田中公美子, 西山勝廣. TiB_2–CeB_6 系複合セラミックスの創製と機械的性質. 粉体および粉末冶金. 2015;62(1):10–17.